



**HAL**  
open science

## Swift heavy ion irradiation of CaF<sub>2</sub> – from grooves to hillocks in a single ion track

Elisabeth Gruber, Pierre Salou, Lorenz Bergen, Mourad El Kharrazi, Elie Lattouf, Clara Grygiel, Yuyu Wang, Abdenacer Benyagoub, Delphine Levavasseur, Jimmy Rangama, et al.

► **To cite this version:**

Elisabeth Gruber, Pierre Salou, Lorenz Bergen, Mourad El Kharrazi, Elie Lattouf, et al.. Swift heavy ion irradiation of CaF<sub>2</sub> – from grooves to hillocks in a single ion track. *Journal of Physics: Condensed Matter*, 2016, 28 (40), pp.405001. 10.1088/0953-8984/28/40/405001 . hal-03190086

**HAL Id: hal-03190086**

**<https://normandie-univ.hal.science/hal-03190086v1>**

Submitted on 31 May 2022

**HAL** is a multi-disciplinary open access archive for the deposit and dissemination of scientific research documents, whether they are published or not. The documents may come from teaching and research institutions in France or abroad, or from public or private research centers.

L'archive ouverte pluridisciplinaire **HAL**, est destinée au dépôt et à la diffusion de documents scientifiques de niveau recherche, publiés ou non, émanant des établissements d'enseignement et de recherche français ou étrangers, des laboratoires publics ou privés.



Distributed under a Creative Commons Attribution 4.0 International License

PAPER • OPEN ACCESS

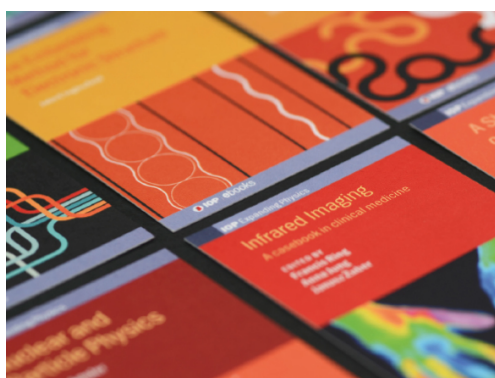
## Swift heavy ion irradiation of $\text{CaF}_2$ – from grooves to hillocks in a single ion track

To cite this article: Elisabeth Gruber *et al* 2016 *J. Phys.: Condens. Matter* **28** 405001

View the [article online](#) for updates and enhancements.

You may also like

- [Controlled morphological modifications of ZnO thin films by ion irradiation](#)  
Vidya Kondkar, Deepti Rukade, Dinakar Kanjilal *et al.*
- [Surface nanostructures on Nb-doped  \$\text{SrTiO}\_3\$  irradiated with swift heavy ions at grazing incidence](#)  
N Ishikawa, Y Fujimura, K Kondo *et al.*
- [Experimental evidence of crystalline hillocks created by irradiation of  \$\text{CeO}\_2\$  with swift heavy ions: TEM study](#)  
N Ishikawa, N Okubo and T Taguchi



**IOP | ebooks™**

Bringing together innovative digital publishing with leading authors from the global scientific community.

Start exploring the collection—download the first chapter of every title for free.

# Swift heavy ion irradiation of CaF<sub>2</sub> – from grooves to hillocks in a single ion track

Elisabeth Gruber<sup>1</sup>, Pierre Salou<sup>2</sup>, Lorenz Bergen<sup>1</sup>, Mourad El Kharrazi<sup>3</sup>,  
 Elie Lattouf<sup>2</sup>, Clara Grygiel<sup>2</sup>, Yuyu Wang<sup>4</sup>, Abdenacer Benyagoub<sup>2</sup>,  
 Delphine Levavasseur<sup>2</sup>, Jimmy Rangama<sup>2</sup>, Henning Lebius<sup>2</sup>,  
 Brigitte Ban-d'Etat<sup>2</sup>, Marika Schleberger<sup>3</sup> and Friedrich Aumayr<sup>1</sup>

<sup>1</sup> TU Wien, Institute of Applied Physics, 1040 Vienna, Austria

<sup>2</sup> CIMAP (CEA-CNRS-ENSICAEN-UCBN), 14070 Caen Cedex 5, France

<sup>3</sup> Fakultät für Physik and CENIDE, Universität Duisburg-Essen, 47048 Duisburg, Germany

<sup>4</sup> Chinese Academy of Sciences, Institute of Modern Physics, 730000 Lanzhou, People's Republic of China

E-mail: [egruber@iap.tuwien.ac.at](mailto:egruber@iap.tuwien.ac.at)

Received 14 June 2016, revised 11 July 2016

Accepted for publication 11 July 2016

Published 12 August 2016



## Abstract

A novel form of ion-tracks, namely nanogrooves and hillocks, are observed on CaF<sub>2</sub> after irradiation with xenon and lead ions of about 100 MeV kinetic energy. The irradiation is performed under grazing incidence (0.3°–3°) which forces the track to a region in close vicinity to the surface. Atomic force microscopy imaging of the impact sites with high spatial resolution reveals that the surface track consists in fact of three distinct parts: each swift heavy ion impacting on the CaF<sub>2</sub> surface first opens a several 100 nm long groove bordered by a series of nanohillocks on both sides. The end of the groove is marked by a huge single hillock and the further penetration of the swift projectile into deeper layers of the target is accompanied by a single protrusion of several 100 nm in length slowly fading until the track vanishes.

By comparing experimental data for various impact angles with results of a simulation, based on a three-dimensional version of the two-temperature-model (TTM), we are able to link the crater and hillock formation to sublimation and melting processes of CaF<sub>2</sub> due to the local energy deposition by swift heavy ions.

Keywords: swift heavy ions, grazing incidence, nanostructure formation, CaF<sub>2</sub>

(Some figures may appear in colour only in the online journal)

## 1. Introduction

The formation of surface nanostructures due to single ion impact is an intriguing phenomena in ion-surface interaction [1–8]. Swift heavy ion (SHI) as well as slow highly charged ion (HCI) irradiations show similarities in the nanostructure formation on different materials despite of the different primary excitation processes involved. While HCIs deposit their potential energy to the topmost atomic layers, SHIs transfer

their energy by ionization and electronic excitation processes (electronic stopping) to the bulk and surface of the irradiated material. The subsequent energy transfer from the electronic to the lattice system leads to damage as well as material modifications at the impact site in the form of nanohillocks or craters (for a recent review see [9]). For the ionic crystal CaF<sub>2</sub>, which is interesting for various applications in microelectronic and optoelectronic devices [10, 11], a large data set from different irradiation experiments is available which shows the creation of nanosized hillocks due to SHI and HCI irradiation under normal ion impact. For HCI irradiation of CaF<sub>2</sub> a so called phase-diagram [8] could be elaborated. It shows that hillock formation is only possible above a certain potential energy



Original content from this work may be used under the terms of the [Creative Commons Attribution 3.0 licence](https://creativecommons.org/licenses/by/3.0/). Any further distribution of this work must maintain attribution to the author(s) and the title of the work, journal citation and DOI.

threshold of 12–14 keV. There the high energy deposition of HCI leads to melting of a nano-sized region around the impact site, followed by thermal expansion and rapid quenching, leading to permanent surface modifications in the form of small nanohillocks [12]. At considerably higher potential energies a further threshold has been predicted [13], above which sublimation/evaporation of atoms and clusters should occur. Since SHIs create similar nanostructures as HCIs [9], in this contribution we investigate nanostructure formation due to SHI irradiation, for which higher energy deposition is more easily achieved than via production of HCI in really high charge states. The SHI irradiation is performed under grazing incidence since this particular collision geometry forces the track to a region close to the surface comparable to the shallow damage of slow HCI.

The occurrence of nanohillocks induced by SHI on CaF<sub>2</sub> under normal incidence was first reported in 2002 by Müller *et al* [14]. These authors showed that the hillock height increases almost linearly with increasing energy loss reaching a height of 13 nm at 35 keV nm<sup>-1</sup>. Further systematic studies [15–17] confirmed these observations and determined an energy loss threshold for hillock creation between  $S_e = 2.3\text{--}5.8$  keV nm<sup>-1</sup>. A similar energy loss threshold was found when measuring the CaF<sub>2</sub> volume expansion (swelling) [18] due to SHI irradiation. First AFM images of CaF<sub>2</sub> irradiated under grazing incidence were presented by Akcöltekin *et al* [19] and showed the creation of chains of single nanodots as already reported before for other materials like SrTiO<sub>3</sub> and TiO<sub>2</sub> [6, 19, 20]. Eddy current microscopy (ECM) measurements of the irradiated CaF<sub>2</sub> samples indicated that the produced nanodots predominantly consist of metallic Ca [21]. This observations suggested a depletion of fluorine, resulting in Ca colloids and were in good agreement with earlier transmission electron microscope measurements that showed the creation of intermittent tracks, consisting of aligned anion voids (or rather calcium inclusions) after irradiation with clusters of ions of a few tens of MeV [22]. The authors of [19] noted the limited spatial resolution of the AFM measurements of the tracks produced on CaF<sub>2</sub> because of the tip radius (convolution) and problems arising from the reactivity of the samples under ambient conditions, which causes the formation of adsorbate islands around the surface tracks, which eventually cover the whole sample and make prolonged measurements difficult.

In this contribution we show that heating of the CaF<sub>2</sub> surface under vacuum conditions largely prevents adsorbate island formation under ambient conditions. Using an AFM instrument with superior resolution, we are able to reveal a more complicated track structure on CaF<sub>2</sub> due to SHI impact than observed so far (section 3). To interpret our results we successfully apply a three dimensional extension of the two-temperature-model (section 4).

## 2. Experimental procedure

The irradiations have been performed at the IRRSUD beamline of GANIL, Caen, France. *Ex situ* cleaved CaF<sub>2</sub> (111) crystals (Crystec, Korth) have been irradiated with

$\sim 100$  MeV <sup>208</sup>Pb<sup>29+</sup> ( $S_e = 18$  keV nm<sup>-1</sup>) or  $\sim 95$  MeV <sup>136</sup>Xe<sup>23+</sup> ( $S_e = 16$  keV nm<sup>-1</sup>) under grazing angles of incidence, with  $S_e$  being the electronic stopping power calculated with SRIM [23]. The charge states of the used ions are close to the respective equilibrium charge states [24]. The targets were mounted on a vertical target holder, which could be rotated around the vertical axis by a stepping motor. The angle of incidence, measured with respect to the surface plane, was varied between 0.3° and 3° with an accuracy of 0.2° [7]. In order to avoid overlapping of individual ion tracks an ion fluence between  $1 \times 10^{10}$  ions cm<sup>-2</sup> and  $5 \times 10^{10}$  ions cm<sup>-2</sup>, depending on the incident angle, was chosen, leading to  $\sim 5$  tracks per  $\mu\text{m}^2$ . After irradiation the samples were immediately inspected with a VEECO NanoScope III atomic force microscope in Caen. For more detailed investigation the samples were transferred to Vienna and studied with an Asylum Research Cypher Scanning Probe Microscope in tapping mode under ambient conditions. As probes, standard Si cantilevers OMCL-AC240TS-R3 (Olympus) with a resonance frequency of 70 kHz and a spring constant of 1.7 N m<sup>-1</sup> were used. Since the observed tracks are a convolution between the real topography and the tip, the AFM images were first unfolded with the software WSxM [25] by assuming a tip radius of curvature of 7 nm and afterwards evaluated with the software Gwyddion [26].

## 3. Experimental results

The 3D plot of figure 1 shows the typical topography of a CaF<sub>2</sub> surface after swift heavy ion irradiation under grazing incidence of 1.3°. It shows the creation of several parallel arranged tracks induced by individual ion impacts. The arrow indicates the direction of the incoming ions. The irradiation induced damage on CaF<sub>2</sub> remarkably differs from the modification previously observed on other insulating materials (SrTiO<sub>3</sub>, TiO<sub>2</sub>, Al<sub>2</sub>O<sub>3</sub>, SiO<sub>2</sub> [6, 7, 19]). The enlarged figure next to the 3D plot shows a detailed picture of one of the created tracks. At the impact site a  $\sim 400$  nm long groove, bordered by a series of nanohillocks on both sides, is created. The end of the groove is marked by a single huge hillock which is followed by a protrusion of several 100 nm length. Longitudinal and cross profiles at various positions of the track enable the analysis of the height, depth and width of the created nanostructures, some examples are plotted in figure 1. The longitudinal profile (a) through the center of the track shows the formation of a groove at the impact site with a depth of 1–2 nm, terminated by a huge single hillock of 14 nm, which is followed by a decaying protrusion of some nm height. Profile (b) is shifted from the center towards one of the chains of the single nanohillocks. It shows a series of equally spaced nanodots with increasing height up to  $\sim 5$  nm which eventually merge into the huge single nanodot at the end of the groove. The profile line to the right of this hillock demonstrates nicely the flatness of the CaF<sub>2</sub> sample (RMS-roughness = 0.15 nm). The cross sections (c) and (d) through the former part of the track show the formation of single nanodots on the right and left side of the groove with a distance of  $\sim 15$  nm in between.

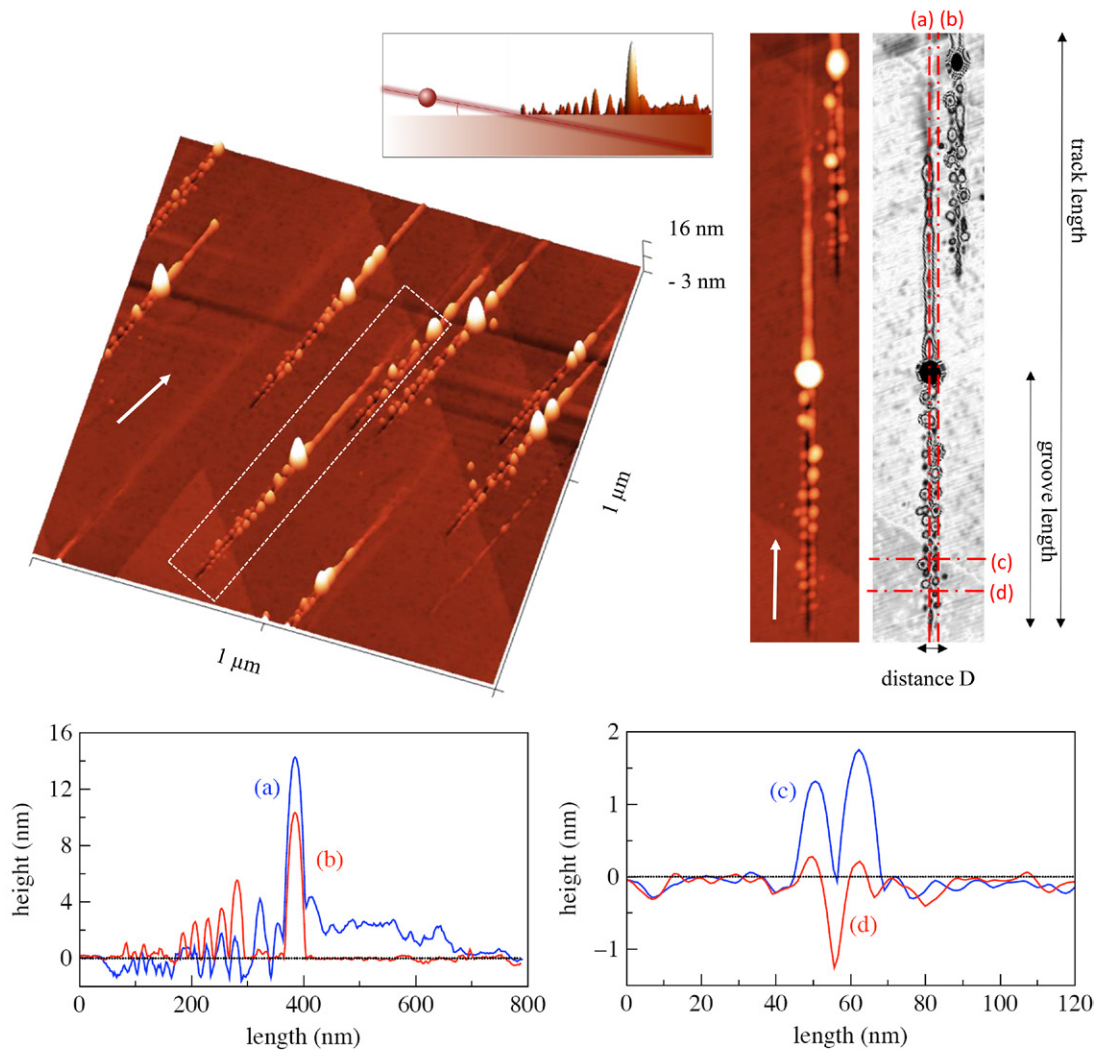


**Figure 1.** 3D plot (upper left) of an AFM image of a  $\text{CaF}_2$  surface irradiated with  $\sim 100$  MeV Pb ions under  $1.3^\circ$  angle of incidence, showing a typical topography of  $\text{CaF}_2$  after individual SHI irradiation under grazing incidence. The white arrows indicate the direction of the incoming ions. The highlighted track is shown in more detail in the figure to the right. At the impact site a long groove bordered by series of nanohillocks is created. The end of the groove is marked by a single huge hillock, followed by a protrusion of several 100 nm length. The dashed lines in the gray image indicate where line profiles shown below have been taken. The longitudinal profiles (a) and (b) and the cross sections (c) and (d) show the size and shape of this single nanotrack (see text).

As mentioned before [19], AFM measurements on  $\text{CaF}_2$  might be challenging due to the formation of adsorbate islands. Adsorption is enhanced in the vicinity of defects and tracks. Under UHV conditions the morphology of the surface is stable and does not change even after days [27]. However, *in situ* AFM measurements of irradiated samples are tedious and require dedicated equipment often not available at beamlines. During our measurements the adsorbate island formation with time was obvious. Figure 2(a) shows an unirradiated sample stored in air 28 h after cleaving where the formation of these islands is clearly visible. Also on an irradiated sample (figure 2(b)) these islands are clearly visible some days after irradiation. When repeating the AFM measurements ten months later, roughly the whole sample is covered (figure 2(c)) by adsorbates. Nevertheless the ion induced nanotracks are still observable. In the course of our investigations we have found a surface preparation technique, which largely prevents the formation of these adsorbate islands.

Heating the cleaved samples to  $400^\circ\text{C}$  under high vacuum conditions ( $10^{-6}$  mbar) for a prolonged time (several hours), seems to make the morphology of the surface stable even under subsequent exposition to air. Figures 2(d)–(f) show such a pretreated  $\text{CaF}_2$  surface before (d), some days (e) and 10 months (f) after irradiation at room temperature. A possible explanation for the stabilization of such pretreated surface is that at moderate temperatures up to  $240^\circ\text{C}$ , defects like H and F centers diffuse within the bulk towards the surface, leading there to fluorine desorption and F center aggregation into metallic colloids [28, 29]. The metallic colloids progressively oxidize or hydroxylize by oxygen and water, therefore forming islands. By heating the crystal well above  $250^\circ\text{C}$ , the evaporation temperature for calcium is surpassed, the surface metal (Ca colloids) is evaporated and an inert and stoichiometric  $\text{CaF}_2$  surface is formed. On perfect  $\text{CaF}_2$  surfaces water molecules do not adsorb at room temperature [30].

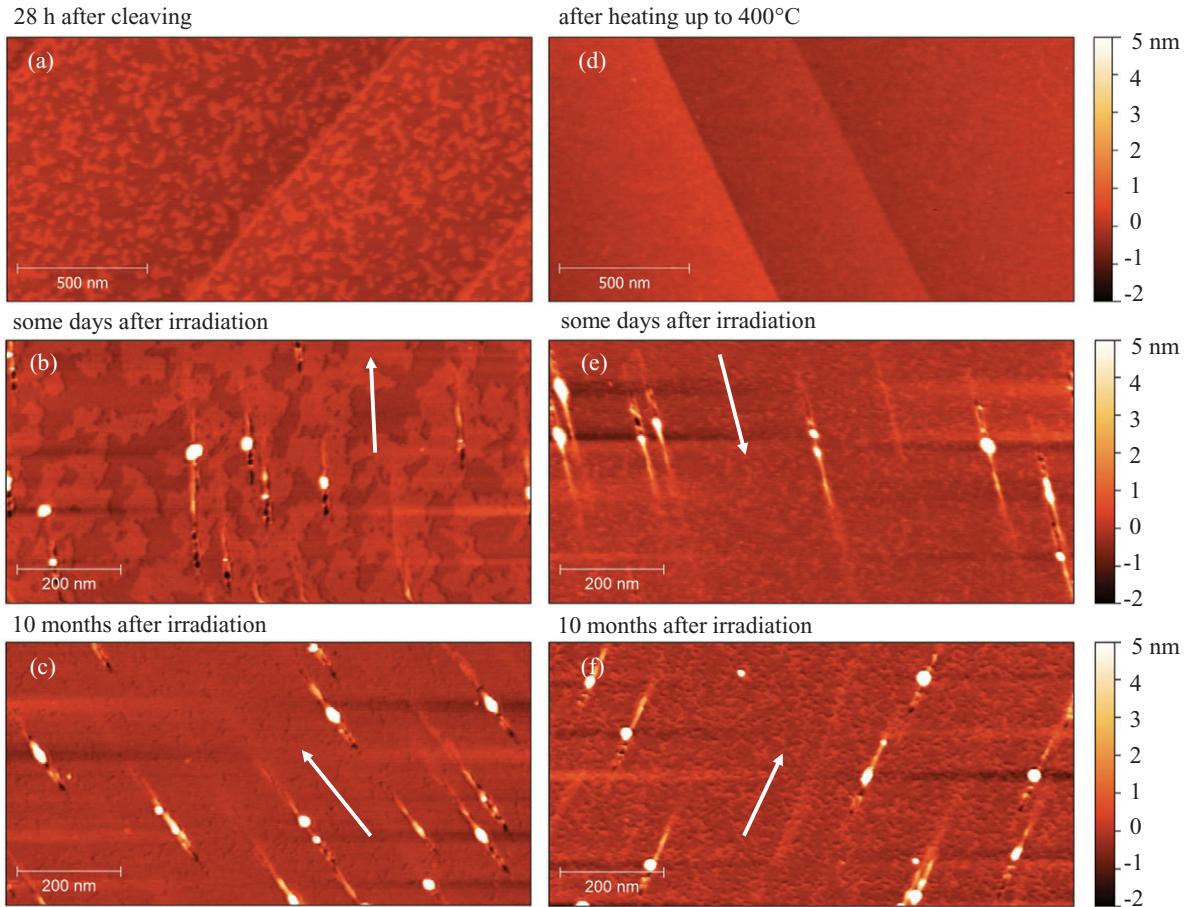


**Figure 2.** AFM images of unirradiated ((a) and (d)) and irradiated ((b), (c), (e) and (f))  $\text{CaF}_2$  samples without pretreatment ((a)–(c)) and after pretreatment by heating to  $400^\circ\text{C}$  before irradiation ((d)–(f)). The irradiations were performed with  $95\text{ MeV }^{136}\text{Xe}^{23+}$  ions. While on the untreated samples the growing of adsorbate islands can be observed with time, the surface morphology of the heated samples seems to be stable for an extended period of time.

Although this is only a tentative explanation for the positive effect of sample heating on adsorbate island formation, we found that the surface morphology and the induced tracks remain stable over an extended period of time. Some properties, like the height and the volume of the single nanodots, may change slightly with time due to the variation of the surface morphology and depend on the imaging mode as well, see [16]. But other properties such as the length of the groove or the length of subsequent track and the distance between the single nanodots of the chains remain the same and are therefore discussed in more detail in the next paragraph.

As reported previously for other materials like  $\text{SrTiO}_3$  [19, 27], also for  $\text{CaF}_2$  the length of the ion track can be controlled by varying the incident angle. As can be seen from figure 3 both, the length of the groove as well as the length of the whole track (for definition see figure 1), follow the relation  $L = d/\tan(\alpha)$  when varying the impact angle from  $0.3^\circ \leq \alpha \leq 3^\circ$  in our experiment. This relation is simply motivated by a geometrical consideration, where  $L$  is the track/groove length and  $d$  the maximum depth from which this particular ion induced modification can still be detected at the surface. From such a fit the characteristic depth for the groove formation is evaluated to be around  $d = 4.8\text{ nm}$  while for the whole track length a value of  $d = 10.6\text{ nm}$  is found. The single hillocks along the

borders of the groove are periodically arranged and their distance also follows a similar  $a/\tan(\alpha)$  relation with the value of  $a$  being close to the lattice constant of  $5.462\text{ \AA}$  (see figure 3).

#### 4. Discussion

The SHI induced damage created on  $\text{CaF}_2$ , more precisely the created grooves surrounded by hillocks followed by a single protrusion, differs from the nanostructure formation on other materials. The chain of single nanodots on  $\text{SrTiO}_3$  and  $\text{TiO}_2$  could be successfully interpreted as remnants of molten zones from rapidly quenched thermal spikes and the appearance of equidistant nanodots attributed to the fact that the ions cross regions with varying electron density [6]. Recently, for  $\text{SrTiO}_3$  a so called rift directly in front of the hillock chain has been reported [31], similar to the rifts found in  $\text{SiC}$  [7]. In contrast to the case of  $\text{CaF}_2$ , the rifts were not bordered by hillocks.

From our AFM measurements of  $\text{CaF}_2$ , which show the formation of a deep groove with bordered hillocks along the impacting trajectory, we conclude that not only melting but also sublimation processes become relevant for this particular track formation. When a SHI with sufficient kinetic energy passes through material, several processes take place on

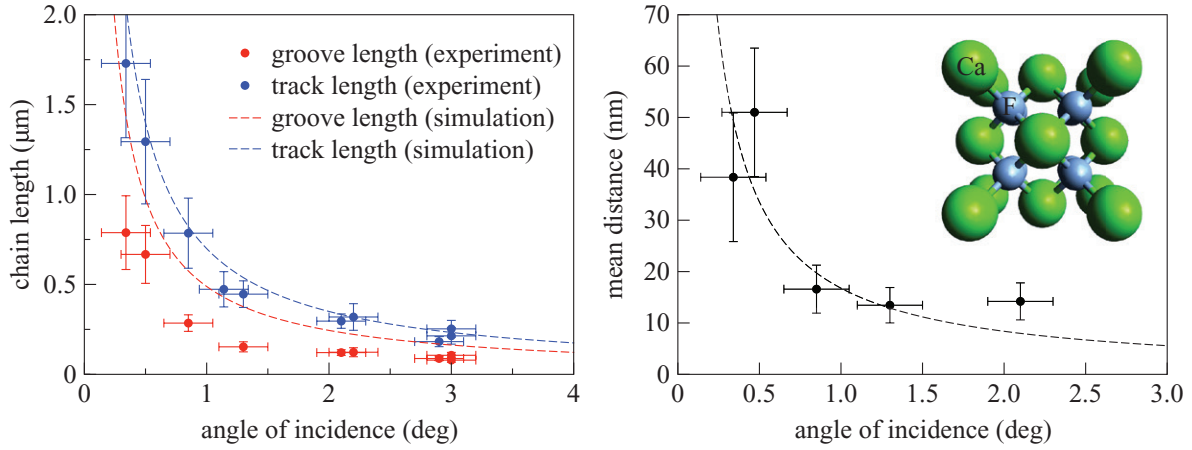


**Figure 3.** Left figure: measured length of groove (orange data points) and length of the whole track (blue data points) as a function of the incidence angle for irradiation with  $\sim 95$  MeV  $\text{Xe}^{23+}$  ions. The dashed lines show the results of the 3D-TTM calculation (see text). The experimental groove lengths are compared to the calculated values of the extension of the surface region where the sublimation temperature is surpassed, while the measured track lengths are compared to the regions where the melting temperature is reached. Right figure: experimentally determined distance (gray data points) between the periodically arranged single nanodots of a chain (see figure 1, in particular the longitudinal profiles (a) and (b) bordering the groove). The experimental data follow the relation  $a/\tan(\alpha)$  with  $a$  being close to the lattice constant  $5.462 \text{ \AA}$  (gray dashed line).

different time scales: in the first fractions of a femtosecond the projectile energy is deposited into the electronic system by excitation and ionization processes, in the following several 100 femtoseconds the energy dissipates from the electronic to the lattice system and in the next ten picoseconds (or more) target material is restructured due to lattice dynamics.

To check if and at which locations the lattice temperature of the irradiated  $\text{CaF}_2$  samples due to energy deposition of the incident ions actually surpasses the sublimation temperature necessary for groove formation, and where the melting temperature for hillock formation, calculations based on the two-temperature-model (TTM) [32, 33] have been performed. The TTM is based on two coupled heat diffusion equations, one for the electron and one for the phonon system, in which the electron–phonon coupling parameter  $g$  controls the energy transfer from the electronic to the lattice system. Since the irradiations have been performed under grazing angle of incidence and the cylindrical symmetry assumed in the conventional TTM is therefore broken, a fully three-dimensional version of the TTM had to be used [7, 34]. In order to compare our experimental data, we chose an incidence angle of  $0.5^\circ$  by setting up a simulation box with length  $x_{\text{box}} = 3000 \text{ nm}$ , width  $y_{\text{box}} = 50 \text{ nm}$  and depth  $z_{\text{box}} = 50 \text{ nm}$ . The simulation box is surrounded by a thermal bath with van Neumann boundary conditions for the surface. Inside the simulation box, the two equations

$$C_e(T_e) \cdot \frac{\partial T_e}{\partial t}(\vec{r}, t) = \nabla \cdot (\kappa_e(T_e) \nabla T_e(\vec{r}, t)) - g \cdot (T_e(\vec{r}, t) - T_p(\vec{r}, t)) + S(\vec{r}, t)$$

$$C_p(T_p) \cdot \frac{\partial T_p}{\partial t}(\vec{r}, t) = \nabla \cdot (\kappa_p(T_p) \nabla T_p(\vec{r}, t)) + g \cdot (T_e(\vec{r}, t) - T_p(\vec{r}, t))$$

are solved. The subscripts e and p refer to electron and phonon quantities, respectively.  $T(\vec{r}, t)$  are the temperatures,

$C(T)$  and  $\kappa(T)$  are the heat capacity and thermal conductivity, respectively. For the lattice as well as for the electrons we use the relation  $\kappa = D \times C$  with  $D$  being the diffusivity. For the phonons  $\kappa_p$  can then be calculated from  $D_p \times C$  with a constant lattice diffusion of  $D_p = 0.368 \text{ \AA}^2 \text{ fs}^{-1}$ . For the electrons we assume that the passing ion will on average excite one electron per  $\text{CaF}_2$  molecule into the conduction band of  $\text{CaF}_2$  with a mean free path of  $\lambda_e = 10 \text{ \AA}$ . Based on the free electron gas, we can calculate the electron density and the Fermi velocity  $v_F = h/(m_e \lambda_F)$ , respectively. The electronic heat capacity can then be calculated with the diffusivity given by  $D_e = 1/3 \lambda_e v_F$ . The electron–phonon-coupling constant  $g = 1.2 \times 10^{19} \text{ J (sm}^3\text{K)}^{-1}$  was calculated from the bandgap of  $\text{CaF}_2$  with a value of  $11.8 \text{ eV}$ . For the source term  $S(\vec{r}, t)$  we used the expression of Waligorski [35] using a mean ionization potential of  $0.137 \text{ keV}$  corresponding to the stoichiometry of  $\text{CaF}_2$ .

The calculations provide a temperature profile of the surface and the bulk of  $\text{CaF}_2$  after SHI impact under grazing incidence. Figure 4 shows the top-view and side-view of the sample temperature 100 fs and 1 ps after ion impact, respectively. The highlighted temperatures of  $1691 \text{ K}$  and  $2806 \text{ K}$  mark the region in which the melting and the sublimation temperature of  $\text{CaF}_2$  is surpassed. To compare the results of the simulation with our experimental findings, calculations under different incident angles have been executed. The extension of the surface region, where the sublimation/melting temperature of  $\text{CaF}_2$  is surpassed, is compared with the experimental values found for the groove and track length respectively. In figure 3 both, the experimental and the simulation results are compared. While the experimental and simulated data for the total track length are in good agreement, the simulation data overestimate the groove length. This could be due to the omission of the latent heat from the calculation or the rather asymmetric track formation. At the ‘impact site’ the target atoms gain enough energy to be ejected from the

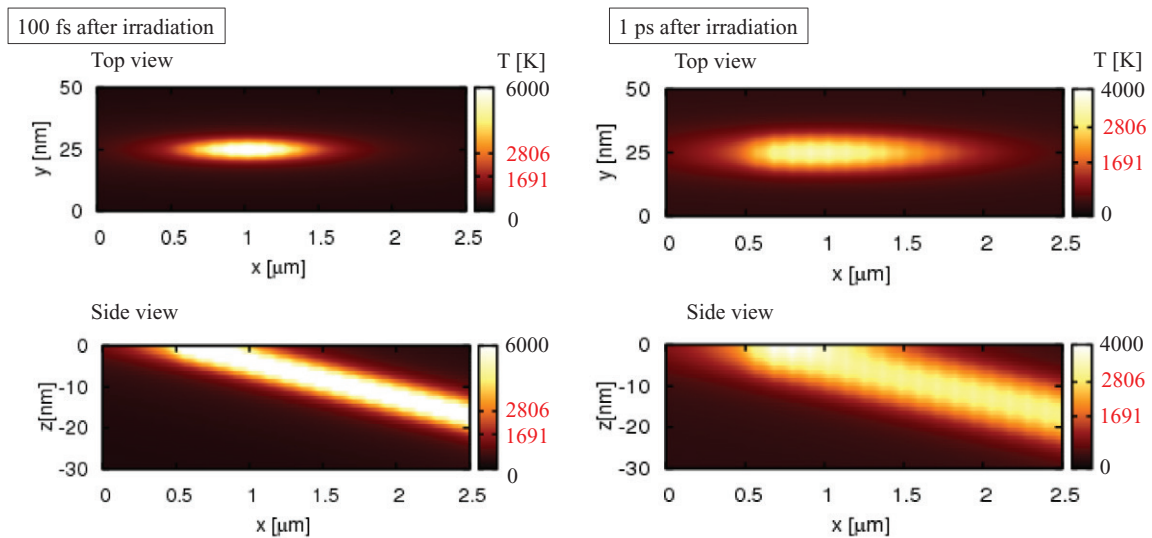


**Figure 4.** Typical results of the 3D-TTM calculation: top-view and side-view of the lattice temperature profile of a  $\text{CaF}_2$  sample 100 fs and 1 ps after ion impact of 95 MeV  $\text{Xe}^{23+}$  ( $S_e = 16 \text{ keV nm}^{-1}$ ) under grazing incidence of  $0.5^\circ$ . The highlighted temperatures of 1691 K and 2806 K mark the region in which the melting and the sublimation temperature of  $\text{CaF}_2$  is surpassed.

surface. Sublimation leads to groove formation. Around the hot zone, where only the melting temperature is surpassed, melting, followed by thermal expansion and rapid quenching, leads to hillock formation. As stated for other materials [6, 20], the creation of a chain of nano-sized hillocks during SHI irradiation at grazing angles of incidence is coupled to the spatially inhomogeneous electron density of the material. Every time the projectile travels through a region of high electronic density, energy can effectively be deposited into the electronic system. Since the electron density corresponds to the periodicity of the crystal, the formation of equidistant hillocks has to be expected.

The deeper the ions penetrate the bulk, the less target atoms can leave the surface. More deeper layers are molten and push material towards the surface, thus filling the initial groove with material. An increase of the hillock height, surrounding the hot zone, is visible which eventually combine to one single huge hillock. Further penetration of the swift projectile into deeper layers of the target is accompanied by a single long protrusion from the (quenched) thermal expansion, which slowly fades until the track vanishes. As a further agreement between measurements and simulation we note that the distance  $D$  between the two chains of hillocks (for details see figure 1) corresponds well with the calculated lateral extension of the melt zone of  $\sim 10\text{--}15 \text{ nm}$  (see top view images of figure 4 and also [36]).

The simulations therefore show that target regions in which the sublimation and melting temperature of  $\text{CaF}_2$  is surpassed, are of comparable dimension as the observed tracks. Similar nanostructures were also observed on other materials [19], but due to the lack of detailed imaging no reliable explanation could be given. The next step will be to check the hypothesis by performing irradiations of other materials with SHI and comparing the found nanostructures with the calculated temperatures in the locally heated areas.

## 5. Conclusion

We have shown that SHI irradiation of  $\text{CaF}_2$  leads to a complex form of ion tracks consisting of a long groove bordered by chains of equally spaced nanodots eventually followed by a single chain of unseparated nanodots with a single high hillock at the beginning. The length of the groove as well as the length of the whole nanotrack can be controlled by varying the angle of incidence. The assumption that the grooves and the surrounding hillocks are induced by sublimation and melting processes, respectively, and the following chains are created by molten material from deeper layers pushed towards the surface, is supported by 3D-TTM calculations. Further investigations by experiments and simulations promise a deeper understanding of the fundamental mechanism of ion-solid interaction processes as well as control over the production of this complex form of nanostructure.

## Acknowledgment

The experiments were supported by the French-Austrian collaboration SIISU, co-financed by ANR (France, ANR-12-IS004-0005-01 SIISU) and by Austrian Science Fund (FWF): project number: I1114-N20.

## References

- [1] Fleischer R L, Price P B and Walker R M 1965 *J. Appl. Phys.* **36** 3645
- [2] Chadderton L 2003 *Radiat. Meas.* **36** 13–34
- [3] Toulemonde M, Trautmann C, Balanzat E, Hjort K and Weidinger A 2004 *Nucl. Instrum. Methods B* **216** 1–8
- [4] Papaleo R M, Thomaz R, Gutierrez L I, de Menezes V M, Severin D, Trautmann C, Tramontina D, Bringa E M and Grande P L 2015 *Phys. Rev. Lett.* **114** 118302
- [5] Karlušić M *et al* 2015 *J. Phys. D: Appl. Phys.* **48** 325304

- [6] Akcöltekin E, Peters T, Meyer R, Duvenbeck A, Klusmann M, Monnet I, Lebius H and Schleberger M 2007 *Nat. Nanotechnol.* **2** 290–4
- [7] Ochedowski O, Osmani O, Schade M, Bussmann B K, Ban-d'Etat B, Lebius H and Schleberger M 2014 *Nat. Commun.* **5** 3913
- [8] El-Said A S, Wilhelm R A, Heller R, Facsko S, Lemell C, Wachter G, Burgdörfer J, Ritter R and Aumayr F 2012 *Phys. Rev. Lett.* **109** 117602
- [9] Aumayr F, Facsko S, El-Said A S, Trautmann C and Schleberger M 2011 *J. Phys.: Condens. Matter* **23** 393001
- [10] Smith T III, Phillips J M, Augustyniak W and Stiles P 1984 *Appl. Phys. Lett.* **45** 907–9
- [11] Schowalter L and Fathauer R 1986 *J. Vac. Sci. Technol. A* **4** 1026–32
- [12] El-Said A S et al 2008 *Phys. Rev. Lett.* **100** 237601
- [13] El-Said A S et al 2007 *Nucl. Instrum. Methods B* **258** 167–71
- [14] Müller C, Cranney M, El-Said A S, Ishikawa N, Iwase A, Lang M and Neumann R 2002 *Nucl. Instrum. Methods B* **191** 246–50
- [15] Khalfaoui N, Rotaru C C, Bouffard S, Toulemonde M, Stoquert J P, Haas F, Trautmann C, Jensen J and Dunlop A 2005 *Nucl. Instrum. Methods B* **240** 819–28
- [16] Khalfaoui N, Görlich M, Müller C, Schleberger M and Lebius H 2006 *Nucl. Instrum. Methods B* **245** 246–9
- [17] Wang Y Y et al 2014 *Sci. Rep.* **4** 5742
- [18] Boccanfuso M, Benyagoub A, Schwartz K, Trautmann C and Toulemonde M 2002 *Nucl. Instrum. Methods B* **191** 301–5
- [19] Akcöltekin S, Akcöltekin E, Roll T, Lebius H and Schleberger M 2009 *Nucl. Instrum. Methods B* **267** 1386–9
- [20] Akcöltekin E, Akcöltekin S, Osmani O, Duvenbeck A, Lebius H and Schleberger M 2008 *New J. Phys.* **10** 053007
- [21] Roll T, Meier M, Akcöltekin S, Klusmann M, Lebius H and Schleberger M 2008 *Phys. Status Solidi* **2** 209–11
- [22] Jensen J, Dunlop A and Della-Negra S 1998 *Nucl. Instrum. Methods B* **141** 753–62
- [23] Ziegler J F, Biersack J P and Ziegler M D 2008 *The Stopping and Range of Ions in Matter* (New York: Pergamon) ([www.SRIM.org](http://www.SRIM.org))
- [24] Shima K, Kuno N, Yamanouchi M and Tawara H 1992 *At. Data Nucl. Data Tables* **51** 173–241
- [25] Horcas I, Fernandez R, Gomez-Rodriguez J M, Colchero J, Gomez-Herrero J and Baro A M 2007 *Rev. Sci. Instrum.* **78** 013705
- [26] Klapetek P, Nečas D and Anderson C Gwyddion user guide (<http://gwyddion.net>)
- [27] Akcöltekin S, Roll T, Akcöltekin E, Klusmann M, Lebius H and Schleberger M 2009 *Nucl. Instrum. Methods B* **267** 683–6
- [28] Bennewitz R, Günther C, Reichling M, Matthias E, Vijayalakshmi S, Barnes A V and Tolk N H 1995 *Appl. Phys. Lett.* **66** 320
- [29] Bennewitz R, Smith D and Reichling M 1999 *Phys. Rev. B* **59** 8237
- [30] Lehmann A, König G and Rieder K H 1994 *Phys. Rev. Lett.* **73** 3125–8
- [31] Meinerzhagen F, Breuer L, Bukowska H, Bender M, Severin D, Herder M, Lebius H, Schleberger M and Wucher A 2016 *Rev. Sci. Instrum.* **87** 013903
- [32] Kaganov M, Lifshitz I and Tanatarov L 1957 *Sov. Phys.—JETP* **4** 173–8
- [33] Toulemonde M, Dufour C and Paumier E 1992 *Phys. Rev. B* **46** 14362
- [34] Karlušić M, Akcöltekin S, Osmani O, Monnet I, Lebius H, Jakšić M and Schleberger M 2010 *New J. Phys.* **12** 043009
- [35] Waligorski M, Hamm R and Katz R 1986 *Int. J. Radiat. Appl. Instrum. D* **11** 309–19
- [36] Toulemonde M, Assmann W, Dufour C, Meftah A and Trautmann C 2012 *Nucl. Instrum. Meth. B* **277** 28–39